Need for Speed and Precision: Structural and Functional Specialization in the Cochlear Nucleus of the Avian Auditory System

Journal of Experimental Neuroscience
Volume 12: 1–16

DOI: 10.1177/1179069518815628

Hui Hong[1] and Jason Tait Sanchez[1,2,3]

[1]Roxelyn and Richard Pepper Department of Communication Sciences and Disorders, Northwestern University, Evanston, IL, USA. [2]Department of Neurobiology, Northwestern University, Evanston, IL, USA. [3]The Hugh Knowles Hearing Research Center, Northwestern University, Evanston, IL, USA.

ABSTRACT: Birds such as the barn owl and zebra finch are known for their remarkable hearing abilities that are critical for survival, communication, and vocal learning functions. A key to achieving these hearing abilities is the speed and precision required for the temporal coding of sound—a process heavily dependent on the structural, synaptic, and intrinsic specializations in the avian auditory brainstem. Here, we review recent work from us and others focusing on the specialization of neurons in the chicken cochlear nucleus magnocellularis (NM)—a first-order auditory brainstem structure analogous to bushy cells in the mammalian anteroventral cochlear nucleus. Similar to their mammalian counterpart, NM neurons are mostly adendritic and receive auditory nerve input through large axosomatic endbulb of Held synapses. Axonal projections from NM neurons to their downstream auditory targets are sophisticatedly programmed regarding their length, caliber, myelination, and conduction velocity. Specialized voltage-dependent potassium and sodium channel properties also play important and unique roles in shaping the functional phenotype of NM neurons. Working synergistically with potassium channels, an atypical current known as resurgent sodium current promotes rapid and precise action potential firing for NM neurons. Interestingly, these structural and functional specializations vary dramatically along the tonotopic axis and suggest a plethora of encoding strategies for sounds of different acoustic frequencies, mechanisms likely shared across species.

KEYWORDS: Auditory, nucleus magnocellularis, potassium channels, sodium channels, resurgent sodium current, tonotopy, avian

RECEIVED: August 31, 2018. **ACCEPTED:** November 6, 2018.

TYPE: Review

FUNDING: The author(s) disclosed receipt of the following financial support for the research, authorship, and/or publication of this article: This research was supported by the National Institute on Deafness and Other Communication Disorders (NIDCD; DC013841—JTS) and the Hugh Knowles Hearing Research Center (JTS).

DECLARATION OF CONFLICTING INTERESTS: The author(s) declared no potential conflicts of interest with respect to the research, authorship, and/or publication of this article.

CORRESPONDING AUTHORS: Hui Hong, Roxelyn and Richard Pepper Department of Communication Sciences and Disorders, Northwestern University, Frances Searle Building, 2240 Campus Drive, Evanston, IL 60208, USA.
Email: HuiHong2018@u.northwestern.edu

Jason Tait Sanchez, Roxelyn and Richard Pepper Department of Communication Sciences and Disorders, Northwestern University, Frances Searle Building, 2240 Campus Drive, Evanston, IL 60208, USA. Email: jason.sanchez@northwestern.edu

Introduction to the Avian Auditory Brainstem

Sensory systems of all vertebrates accurately encode important information from the surrounding environment—a process critical for survival and biological functions. This includes the auditory system, which relies on multiple nuclei in the brainstem to accurately encode temporal, frequency, and intensity information of sound. As a result, the auditory brainstem plays a pivotal role in sound localization and signal extraction in complex listening environments.[1,2] For example, barn owls are able to localize the source of a sound with error as small as 1.5° in azimuth. This remarkable ability requires neurons in the auditory brainstem to recognize timing disparities between the two ears as small as 10 μs.[3,4] More surprisingly, these auditory brainstem neurons are also able to follow and phase lock to acoustic inputs up to several thousand hertz.[5–7] In addition to reliable sound localization, newborn ducklings are capable of distinguishing different maternal calls (ie, different temporal patterns and frequencies) and thus imprint on those from the same species only.[8–10] For example, the maternal call of mallard ducks contains frequency information up to 3 kHz.[8] This requires their auditory system to reliably encode high-frequency patterns of sounds. Interestingly, ducklings could not distinguish different maternal calls when their high-frequency hearing was impaired.[9,10] These remarkable hearing abilities require ultrafast and temporally precise encoding of acoustic elements, which are rooted in the highly specialized properties of auditory brainstem neurons that form microcircuits.[11–14] For more than a half of century, the avian auditory brainstem has been used as an excellent model system for studying development, auditory processing, and underlying mechanisms. Nevertheless, most of the studies focused on mid- to high-frequency regions with few exceptions in the homing pigeon and the domesticated chicken.[15,16] These birds can hear sound as low as 2 Hz (ie, infrasound) and as noted by both studies; the bird's perception of low-frequency sound is distinct compared with higher frequency sound. In this review, we discussed several important temporal coding mechanisms in the chicken auditory brainstem, along with the recent insights regarding neural properties for low-frequency sound processing.

Structural Specialization in Nucleus Magnocellularis

Neurons in nucleus magnocellularis (NM)—the avian analogue of bushy cells of the mammalian anteroventral cochlear nucleus (AVCN)—relay peripheral inputs through auditory nerve fibers (Figure 1A). Synapses at NM neurons are highly specialized for information transmission from the peripheral to central auditory system. However, structural specializations differ across the tonotopic axis, indicating diverse sound

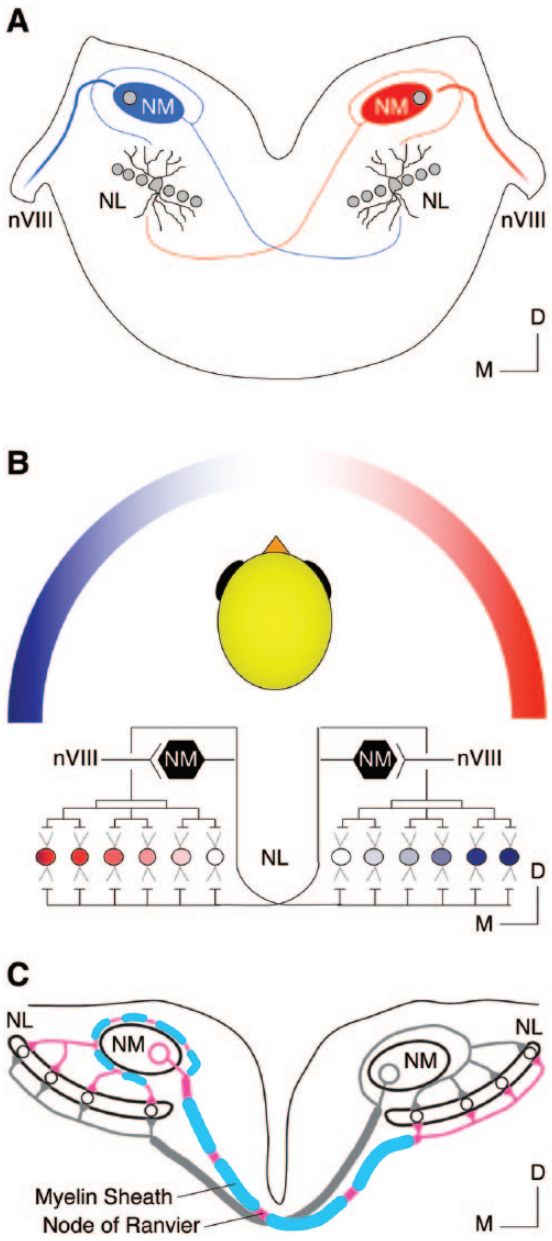

Figure 1. Binaural hearing microcircuit responsible for temporal coding in the avian auditory system. (A) Schematic coronal section of the chicken auditory brainstem. (B) Schematic representation of the neural circuit (ie, modified Jeffress model) in chickens responsible for sound localization. (C) Schematic illustration of NM's projections to NL. Note the difference in myelin between the ipsilateral and contralateral projections. Images in (B) and (C) were modified with permission from Sanchez et al., 2018. D indicates dorsal; M, medial; nVIII, auditory nerve; NL, nucleus laminaris; NM, nucleus magnocellularis.

frequency processing mechanisms. Nucleus magnocellularis neurons send bilateral projections to neurons in nucleus laminaris (NL, Figures 1A to C). Nucleus laminaris, the avian analogue to mammalian medial superior olive (MSO), receives inputs from both ears and functions as a coincidence detector for sound localization. To encode differences in the arrival of sound between the two ears with microsecond precision, microcircuits between NM and NL must also exhibit highly specialized structural organization (Figure 1B and C).

Tonotopic heterogeneity of NM and its auditory nerve inputs

Nucleus magnocellularis neurons are known for their rapid and reliable phase-locking ability to peripheral hearing inputs and thus are able to preserve critical temporal elements of sound information.[17,18] This phase-locking ability is in part attributable to structural specializations of NM. Nucleus magnocellularis neurons are mostly adendritic, and as a result, auditory nerve fibers make direct contact onto the soma of NM neurons via large endbulb of Held synapses (Figure 2A and B, *top*).[19,22] This large synapse contains several release sites of the excitatory neurotransmitter glutamate and ensures the reliable transmission of acoustic information from the auditory nerve to the brainstem.[23,24] The number of release sites per endbulb is not known for birds, but can range from several hundred to more than a thousand sites for mammals.[25] Regardless, NM neurons are able to generate large and extremely fast excitatory postsynaptic currents (EPSCs); the amplitude and speed of which can be as high as 10 nA within 0.5 ms.[26,27] This large and fast synaptic current overcomes the low input resistance of NM neurons (discussed further below), rapidly charges the neuronal membrane, reduces temporal jitter during action potential (AP) generation, and helps maintain the fine structure of sound with minimal time delay.

NM neurons synapse with a small number of non-branching auditory nerve fibers (ie, 1-3 synapses).[28] This anatomical phenotype is functionally significant in terms of high-frequency sound processing. As suggested by a recent modeling study,[29] NM neurons receive a minimal number of synaptic contacts to prevent input convergence and to phase-lock reliably to high-frequency sound. As shown by their model NM neuron, phase-locking to high-frequency sound declined with increasing inputs. They further showed that when synaptic convergence occurred, NM neurons integrated inputs across multiple stimulus periods and resulted in reduced temporal fidelity. Such an observation is further owing to the nature of high-frequency sound, the waveforms of which have extremely brief stimulus periods. Thus, a small number of endbulbs of Held synapses onto individual NM neurons are structural specialization for promoting high-frequency phase-locking.

Despite the traditional view of the endbulb of Held synapse, recent findings demonstrated that this feature is not ubiquitous across the tonotopic axis in birds. The tonotopic axis of NM extends in a caudolateral to rostromedial orientation in the brainstem, with the lowest sound frequencies encoded at the most-caudolateral pole (Figure 2C).[11] In contrast to their higher frequency counterparts, low-frequency NM neurons (chicken, <500 Hz; barn owl, <1000 Hz) in the caudolateral region (termed NMc) show extensive dendritic processes (Figure 2A, *bottom*). Auditory nerve terminals form multiple small bouton synapses onto the dendrites of NMc neurons, instead of the characteristic endbulb of Held synapse (Figure 2B, *bottom*).[19,26,30] In addition, neural response to sound recorded from NMc

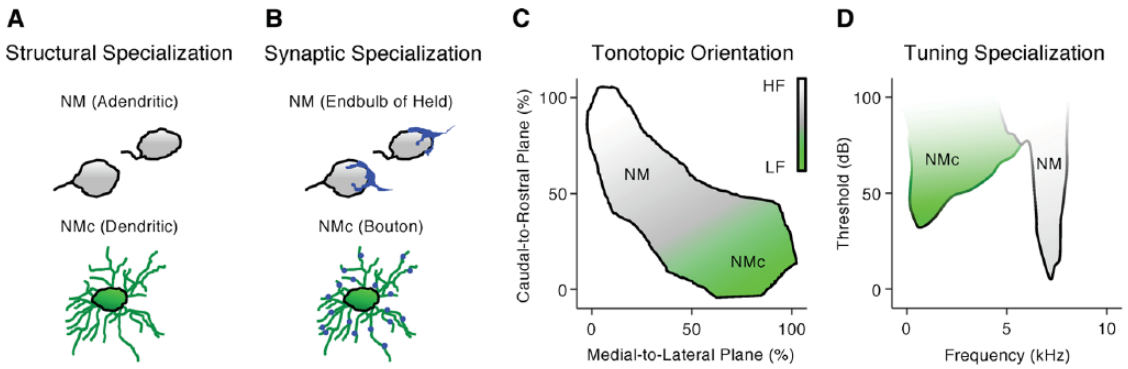

Figure 2. Structural and functional specializations across the tonotopic axis of nucleus magnocellularis (NM). (A, B, and D) Schematic illustrations showing the structural (A), synaptic (B), and tuning (D) differences between mid- to high-frequency NM and low-frequency NM (termed NMc) neurons. Structural and synaptic differences were modified from Wang et al.[19] Tuning differences were modified from Warchol and Dallos.[17,19] (C) Schematic illustrations showing the tonotopic orientation of NM. Tonotopic orientation was modified from Kuba and Ohmori.[21] For simplicity, "NM" in all figures represents the traditionally defined, adendritic NM neurons that are mainly located in mid- to high-frequency region.

region is somewhat different from the rest of NM (ie, mid- to high-frequency NM). Single-unit recordings revealed that ~60% of low-frequency units display frequency tuning curves that resemble a low-pass filter, with the lowest threshold found in response to sound frequency at 10 Hz (Figure 2D).[20] This is notably different from the tuning curves of higher frequency NM, which present a typical "V" shape and resemble a band-pass filter (Figure 2D).[17]

It is worth noting that NMc neurons show excellent phase-locking to low-frequency sound that is comparable to their higher frequency NM counterparts, despite NMc distinct anatomical properties.[20] This suggests different sound processing mechanisms specific to sound frequencies. Computational modeling revealed that multiple-input convergence improves phase-locking to very low-frequency sound.[21,29] Several studies support the idea that input convergence is favorable for NMc neurons. First, NMc neurons receive multiple bouton synapses from the auditory nerve.[19] Second, NMc neurons generate significantly smaller EPSCs (<4 nA) from these small bouton synapses.[26,29] Small EPSCs further elicit subthreshold excitatory postsynaptic potential (EPSP),[21] resulting in the summation of multiple EPSPs essential for AP generation. Third, low-frequency sounds have relatively long stimulus periods. Unlike the aforementioned higher frequency NM neurons, the nature of low-frequency sound allows NMc neurons to integrate information within the same stimulus period that reduces jitter and improves AP phase-locking.[29]

Another important feature of NMc is the heterogeneity of anatomical structures found within this region, in contrast to homogeneous adendritic anatomy of mid- to high-frequency NM. In chickens, NMc region is further divided into NMc1 and NMc2 sub-regions based on their dendritic architecture.[19] NMc2 neurons are categorized by their dramatically longer dendrites and significantly more primary dendritic trees, whereas NMc1 neurons show a medium amount of dendritic processes. NMc1 neurons are located adjacent to the adendritic NM neurons. NMc2 neurons surround the caudal and lateral edges of NMc1 and occupy the most caudal pole of the nucleus. This heterogeneity is also observed in the caudolateral NM of the barn owl, labeled as "sp" and "st" neuronal types.[6]

In summary, NM neurons, including NMc, show specialized anatomical properties that ensure reliable signal transmission from the periphery and precise temporal coding for various sound frequencies, which is fundamental to downstream sound processing (eg, coincidence detection). For simplicity, "NM" in the following text and all figures represents the traditionally defined, adendritic NM neurons that are mainly located in mid- to high-frequency region, while "NMc" denotes the low-frequency neurons with extensive dendrites, including NMc1 and NMc2.

NM projection to NL

Nucleus magnocellularis neurons send well-tuned bilateral projections to NL neurons that resemble what is known as the modified Jeffress model (ie, a neural "place" mechanism to extract timing differences between the two ears) in a discrete tonotopic and topographic fashion.[11,14] As a result, the tonotopic axis of NL shows similar orientation to that of NM. Nucleus laminaris neurons with similar characteristic frequencies are located on the plane orthogonal to the tonotopic axis. In chickens, these NL neurons are aligned as a single-cell sheet, referred here as "isofrequency band." Nucleus laminaris neurons are bipolar and present with segregated dendritic architecture.[13] Axons from the ipsilateral NM synapse onto the dorsal dendrites of NL within the isofrequency band, whereas those from the contralateral side contact the ventral dendrites (Figure 1A and B). *In vitro* recordings demonstrated that NL neurons display maximal response when ipsilateral and contralateral inputs arrive simultaneously.[31,32] Therefore, NL neurons play a major role in detecting "coincidental" arrival of inputs—a critical process for sound localization.

Besides the structural specializations of NL neurons, sophisticated microcircuits between NM and NL enable remarkable

sound localization ability in birds. In chickens, a single axon emerging from each NM neuron first courses ventromedially toward the midline before it bifurcates into ipsilateral and contralateral pathways (Figure 1C). The ipsilateral axon projects dorsolaterally until it reaches the lateral-most edge of NM, where it turns back around toward the ipsilateral NL. This ipsilateral pathway further branches into numerous axons that terminate at the dorsal dendrites of NL.[14] These axon collaterals are approximately equal in length (Figure 1A and C). Therefore, it takes nearly the same amount of time for each NL neuron to receive ipsilateral signals. The contralateral pathway forms the dorsal cochlear tract that crosses the midline and reaches the medial edge of the contralateral NL, where it begins to ramify. In contrast to the ipsilateral pathway, the length of axon collaterals becomes increasingly longer from medial to lateral NL neurons, forming an array of "delay lines" that offset various interaural time differences (ITDs, Figure 1B and C).[14,31] Therefore, within NL, there is an "auditory place map" that represents the horizontal hearing environment as originally proposed by Lloyd Jeffress more than a half century ago.[33]

Recent findings indicate that not only the anatomical delay lines but also the difference in conduction velocity between ipsilateral and contralateral pathways plays an important role in fine-tuning microsecond precision of ITDs.[34,35] This is especially true for the most medial NL neurons, which encode sound coming from straight ahead (ie, ITD = 0 ms). If assuming equal conduction velocity between the two pathways, the ipsilateral input would always arrive earlier than contralateral one due to its shorter distance to travel. To overcome this anatomical limitation requires a remarkable feat of biological engineering. For example, it was recently shown by Seidl et al[34] that the conduction velocity of contralateral axons is more than two-fold larger than ipsilateral axons (~8 vs 3 m/s, respectively). This differential conduction velocity counterbalances the difference in axon length and thus ensures the simultaneous arrival of inputs to the most medial NL neurons. Slower conduction velocity in the ipsilateral axon is a result of significantly shorter internode myelin distance and smaller axon caliber, as compared with the contralateral axon (Figure 1C).[36] This further suggests a mechanism that allows local interaction between axons and surrounding neural structures that undergo myelination. Interestingly, differential internode distance and axon caliber was also observed in axon collaterals from AVCN to MSO in gerbils.[37] Despite morphological similarities, whether there is a conserved sound localization principle across birds and mammals has long been debated.[38] Evidence from guinea pigs includes the role of inhibition and suggests a "two-channel" coding strategy that argues against a Jeffress-like, delayed-line ITD coding system,[39,40] which, by contrary, has been well established in the avian binaural auditory circuit.[41] Regardless, microcircuits from NM to NL are fine tuned in their axon length, caliber, and myelination, to perform accurate ITD computations.

Functional Specialization in NM

Specialized biophysical properties of both NM and NL neurons also serve as key players in promoting precise and rapid encoding of acoustic inputs. On one hand, NM and NL neurons generate extremely fast EPSCs in response to presynaptic release of the neurotransmitter glutamate, with rise and decay times usually less than 1 ms.[27] This rapid EPSC is mediated by α-amino-3-hydroxy-5-methyl-4-isoxazolepropionic acid (AMPA)-type glutamate receptors. On the other hand, intrinsic ion channels regulate fast and reliable generation of APs, the firing pattern of which carries important sound information and propagates successively through the axon. The following focuses on voltage-dependent potassium (K_V) and sodium (Na_V) channels in chicken NM neurons. The properties, function, and development of these ion channels are described in detail.

Function and development of voltage-dependent potassium (K_V) channel

Nucleus magnocellularis neurons show a large amount of outward K_V current with an amplitude up to 5 to 8 nA at positive membrane voltages (Figure 3A and B).[42,44,45] This K_V current is mainly constituted of low- and high-voltage activated components, and both of them show little apparent inactivation with sustained depolarization (Figure 3A and C). Low-voltage activated potassium (K^+_{LVA}) current presents with a half activation voltage ($V_{1/2}$) of −58 mV and is able to activate with extremely fast kinetics, as shown by an activation time constant of <1 ms at most potentials.[45] K^+_{LVA} current is sensitive to dendrotoxin (DTx) and thus is mainly mediated by K_V1 subunits. *In situ* hybridization demonstrated high intensity of $K_V1.1$ and $K_V1.2$ messenger RNA (mRNA) but very weak $K_V1.6$ in NM neurons.[26] In the same study, strong staining of $K_V1.1$ protein was also observed. In contrast to K^+_{LVA}, high-voltage activated potassium (K^+_{HVA}) current shows a less negative $V_{1/2}$ at −19 mV and activates with a slightly slower time constant between 1 and 5 ms.[45] This current is sensitive to tetraethylammonium (TEA) and is mainly mediated by K_V3 subunits. More specifically, intense immunoreactivity of $K_V3.1$ mRNA and proteins were observed in NM neurons.[46] Besides K_V1 and K_V3 subunits, evidence showed that other subtypes of potassium channels, such as K_V2 and calcium-activated BK channels, are minimal in NM neurons (Figure 3C).[44,47,48] Dual application of K_V1 and K_V3 blockers abolished most of outward current in NM neurons.[42] NM neurons also show robust transient A-type potassium current that inactivated rapidly with sustained depolarization (Figure 3A, arrow).[45] The molecular substrates and function of this current are not clear and thus require further investigation. (Note that differences in K_V current, active, and passive properties between mid- to high-frequency NM and low-frequency NMc neurons are shown in Figure 3A to G for comparison purposes, but are discussed in greater detail in the final section of this review.)

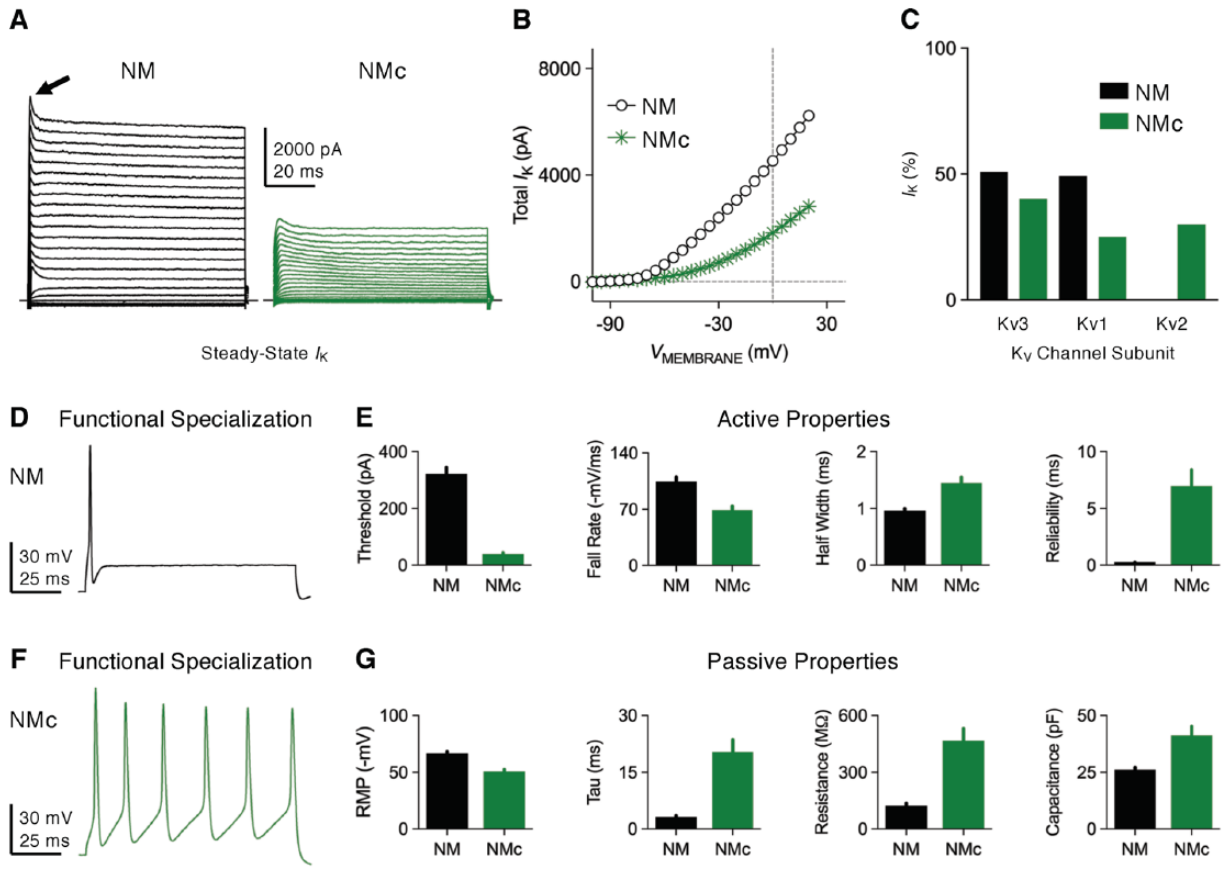

Figure 3. Voltage-dependent potassium (K_V) current properties. (A) Representative K_V current traces recorded from mid- to high-frequency NM and NMc neurons, in response to membrane voltages from –100 mV to +20 mV in a step of 5 mV. Arrow points to transient A-type current. (B) Population data showing the amplitude of steady-state K_V current (I_K) as a function of membrane voltage ($V_{MEMBRANE}$) for the two neuronal groups. (C) Average percent contribution of K_V3-, K_V1-, and K_V2-mediated currents to total K_V current at the membrane voltage of +20 mV. (D and F) Representative membrane responses recorded from mid- to high-frequency NM (D) and NMc (F) neurons to sustained current injection. The amplitude of current injection is 500 and 200 pA, respectively. (E and G) Population data showing the differences in active (E) and passive (G) membrane properties between the two neuronal groups. Reliability is a measure of jitter and was defined as the range of peak occurrences of 30 action potentials (APs). Data were adapted from Hong et al[42,43] and Wang et al.[19] Error bar = standard error. NM indicates nucleus magnocellularis; RMP, resting membrane potential; Tau, time constant.

K^+_{LVA} and K^+_{HVA} channels play important roles in shaping functional phenotypes of NM neurons. A biophysical hallmark of these NM neurons is the generation of a single-onset AP in response to sustained current injection (Figures 3D and 4A, *left*).[42,49] In addition, NM neurons generate extremely fast APs (ie, half width <1 ms) with minimal amounts of jitter (Figure 3E), response properties in stark contrast to the slower, multiple AP generation of NMc neurons (Figure 3E and F).[19,43] When stimulated with square pulse trains of varying frequencies, NM neurons are able to follow the inputs with good fidelity up to 200 Hz at room temperature (22°C-24°C, Figure 4C, *left* and D) and to 500 Hz at near-physiological temperature (38°C-40°C).[48,50] The excitability of the neuron, along with the speed and precision required for AP generation, is partially attributable to K^+_{LVA} and K^+_{HVA} channels. K^+_{LVA} channels activate at resting membrane potential (RMP), regulate the time constant and input resistance of the membrane, and control neuronal excitability. Blockade of K^+_{LVA} by DTx dramatically increases neuronal excitability with little effect on AP kinetics. Nucleus magnocellularis neurons with DTx fire multiple APs in response to sustained current injection and show a large reduction in their threshold current (Figure 4A, *right*). In addition, input resistance is elevated after blockade of K^+_{LVA} and time constant prolonged, which is likely to induce more jitter when generating APs.[26] In contrast, K^+_{HVA} channels activate during APs and contribute to their ultrafast repolarizing kinetics. Blockade of K^+_{HVA} by TEA significantly widens APs and reduces their fall rate (Figure 4B). The widening of APs further undermines neuron's ability to follow high-frequency inputs, such as 200 Hz (Figure 4C, *right* and D). Taken together, both K^+_{LVA} and K^+_{HVA} channels in NM neurons display similar function to those reported in mammalian neurons.[51]

Interestingly, K^+_{LVA} and K^+_{HVA} channels in NM neurons do not develop in parallel with age.[42,52] At embryonic (E) day 12 or younger when chickens are not able to respond to sound (ie, before hearing onset),[53] the total amount of K_V current is significantly less than mature NM neurons, with the amplitude only up to ~3 nA at positive membrane voltages (Figure 5A). K_V current at these early ages is dominated by high-voltage activated

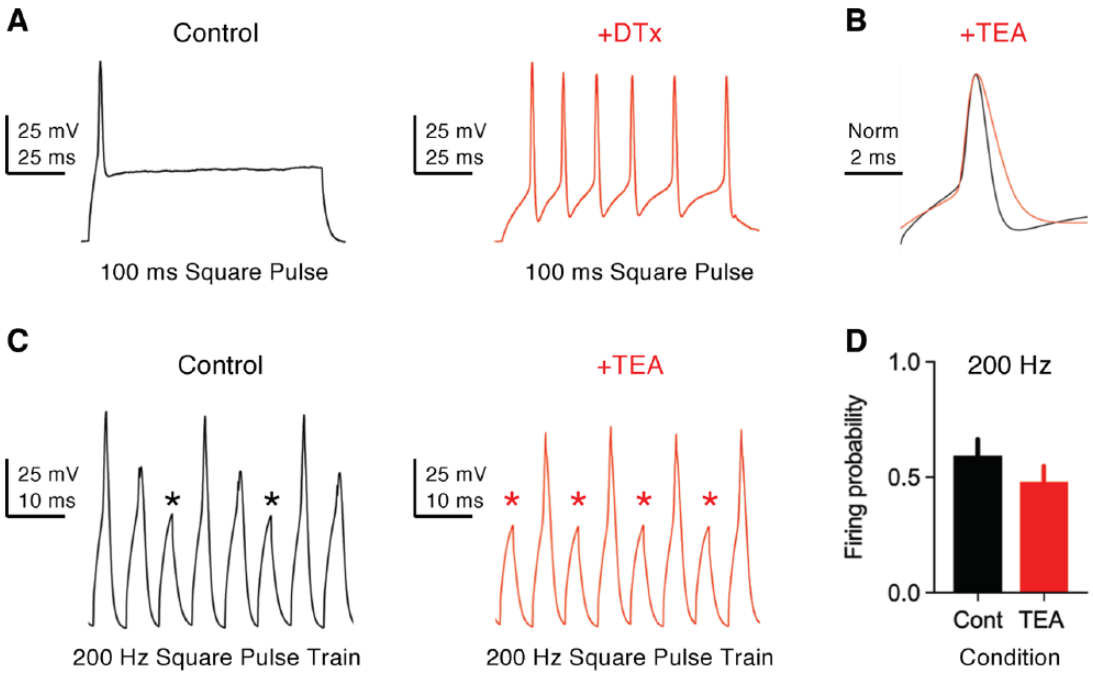

Figure 4. Function of K_V1- and K_V3-containing channels in NM neurons. (A) Representative membrane responses recorded from a mid- to high-frequency NM neuron to sustained current injection (100 ms) in control and with bath application of dendrotoxin (DTx, 0.1 μM). DTx blocks K_V1-containing channels. The amplitude of current injection is 440 pA in control and 60 pA with DTx. (B) Representative APs (normalized) recorded from a mid- to high-frequency NM neuron in control and with bath application of TEA (1 mM). TEA mainly blocks K_V3-containing channels. (C) Representative membrane responses recorded from a mid- to high-frequency NM neuron to square pulse trains of 200 Hz in control and with TEA. Asterisks denote AP failures. (D) Population data showing the difference in firing probability to 200 Hz input. Firing probability was calculated as the number of APs divided by the number of square pulses. Error bar = standard error. Data were adapted from Hong et al.[42,50] APs indicates action potentials; Cont, control; NM, nucleus magnocellularis; TEA, tetraethylammonium.

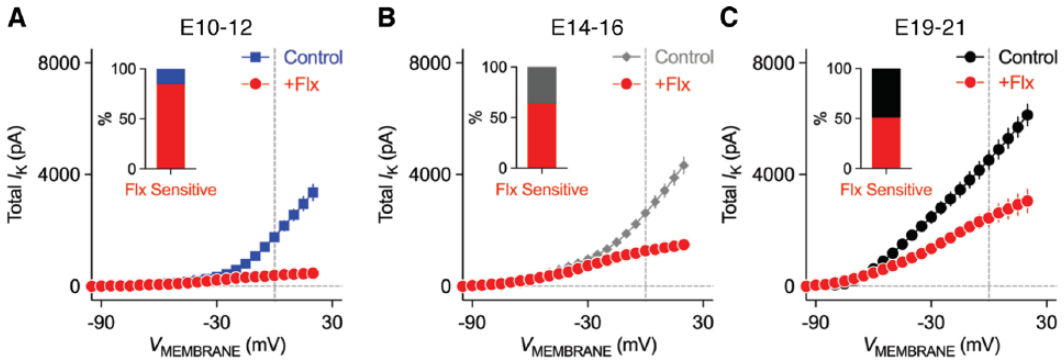

Figure 5. Development of K_V current properties in NM neurons. (A-C) Population data showing the amplitude of K_V current (I_K) as a function of membrane voltage ($V_{MEMBRANE}$) for mid- to high-frequency NM neurons at the age of embryonic (E) days (A) 10-12, (B) 14-16, and (C) 19-21. Fluoxetine (Flx, 100 μM) mainly blocks K_V3-containing channels. Insets showing the percent of K_V current at +20 mV that is sensitive to Flx. Error bar = standard error. Data were adapted from Hong et al.[42] NM indicates nucleus magnocellularis.

components because ~85% of current was eliminated with bath application of fluoxetine (Flx), another potent blocker for K_V3-containing channels (Figure 5A). Consistent with this result, moderate levels of $K_V3.1$ protein expression were observed at E12.[54] At the age of E14 to E16 when chickens show crude response to sound (ie, during hearing onset), the total amount of K_V current increases while the percent of K^+_{HVA} drops to ~64% (Figure 5B). This is because K^+_{LVA} channels start to develop at these ages.[42,49] The development of K^+_{LVA} occurs rapidly and results in a comparable amount of K^+_{LVA} and K^+_{HVA} currents at the age of E19 to E21 (ie, after hearing onset, Figures 5C and 3C). Chickens hatch at E21, and by the time they hatch, near-mature hearing ability is established.[55,56] Nevertheless, a recent study demonstrated that the amount of K^+_{LVA} current further enhanced during chicken's posthatch development, while K^+_{HVA} stayed relatively constant.[52] In summary, K^+_{HVA} channels in NM neurons appear at early embryonic development, whereas K^+_{LVA} channels show some delay in their development until the onset of hearing.

Function and development of voltage-dependent sodium (Na_V) channel

Nucleus magnocellularis neurons show inward transient Na_V current (I_{NaT}) with maximal amplitude between 3 and 5 nA (Figure 6A and B).[21,42] The molecular substrates regarding the α-/β-subunits underlying I_{NaT} in NM remain largely unexplored. However, recent studies revealed intensive expression of $Na_V1.6$ subtypes on the axon of NM neurons, likely clustering at the axon initial segments (Figure 6E, *top* and F).[43,50] Activation of I_{NaT} in NM neurons shows $V_{1/2}$ ~−31 mV with equilibrium potential at +35.8 mV.[44] The voltage dependence of I_{NaT} inactivation shows $V_{1/2}$ ~−55 mV and slope factor (k) ~4.5 mV, which indicates that ~20% of Na_V channels are inactivated at RMP (Figure 6C, *top* and D). (Note that differences in Na_V current between mid- to high-frequency NM and low-frequency NMc neurons are shown in Figures 6A to F, 10A to D, and 11A to H for comparison purposes but are discussed in greater detail in the final section of this review.)

In addition to the important roles of K_V channels, unique properties of I_{NaT} also subserve the rapid AP firing in NM neurons. I_{NaT} shows fast kinetics with a half width ~1 ms.[42] More remarkably, when double-pulse protocol was applied to NM neurons, the amplitude of the second I_{NaT} was able to recover >80% within 3 ms (Figure 7A and B). This recovery rate is visibly faster than those reported in cerebellar Purkinje and nuclear neurons.[57] Therefore, the fast recovery kinetics of I_{NaT} contributes to high-frequency firing capability of NM neurons and is important for performing rapid auditory functions.

The properties of I_{NaT} in NM neurons undergo profound changes with maturation.[42] The amplitude of I_{NaT} increases significantly from E10 to E21 (Figure 8A and B). This increase in amplitude can be divided into two phases separated by the onset of hearing. Between the ages of E10 and E16, the I_{NaT} current density (ie, nA/pF) increases significantly with minimal change in total channel conductance (Figure 8C and D). The current density indicates the number of Na_V channels per unit area and suggests that the increase in I_{NaT} amplitude is attributable to a higher channel expression. In contrast, total channel conductance augments significantly after E16, while current density stays relatively constant (Figure 8C and D). A change in channel conductance suggests the expression of different Na_V channel subtype(s) after hearing onset. Interestingly, our immunochemical results support this idea.[50] The $Na_V1.6$-positive axon segments are absent at E15 and E11 as compared with their robust expression at E21 (Figure 9). Similar results were found in NL neurons, and Na_V channel subtypes switched from $Na_V1.2$ to $Na_V1.6$ around E18.[58] It remains to be determined whether NM neurons also express $Na_V1.2$ subtypes at early embryonic ages.

Accompanying the increase in I_{NaT} amplitude with age are changes in I_{NaT} kinetics and voltage dependence of inactivation. I_{NaT} kinetics improves significantly from E10 to E21 (Figure 8E to G). The voltage dependence of inactivation shows minimal change between E10 and E16 but shifts toward hyperpolarization with significantly more negative $V_{1/2}$ at E19 to E21 (Figure 8H). In summary, the amplitude, kinetics, and voltage dependence of I_{NaT} display significant developmental changes that are likely the combined results of the number and subtypes of Na_V channels.

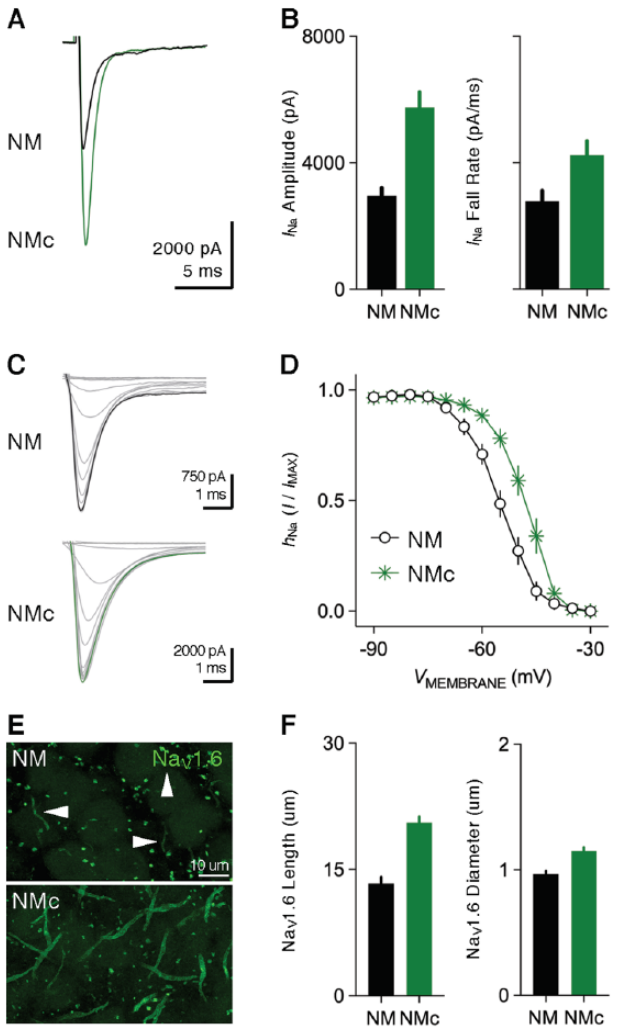

Figure 6. Voltage-dependent sodium (Na_V) current properties. (A) Representative transient Na_V current traces recorded from mid- to high-frequency NM and NMc neurons in response to membrane depolarization at −30 mV. (B) Population data showing the differences in Na_V current (I_{Na}) amplitude and fall rate at the membrane voltage of −30 mV between the two neuronal groups. Both bar graphs share the same scale in Y-axis. (C) Representative Na_V current traces recorded from mid- to high-frequency NM and NMc neurons, in response to depolarization to −30 mV following pre-pulse holding voltages from −90 to −30 mV in a step of 10 mV. (D) Population data showing voltage dependence of Na_V channel inactivation for the two neuronal groups. h_{Na} was calculated as the Na_V current recorded for each trial normalized to the maximum current across all trials and plotted as a function of the holding voltage. (E) High power images with z-projection showing the immunoreactivity of $Na_V1.6$ subtype in mid- to high-frequency NM and NMc regions. Arrowheads point to $Na_V1.6$-positive axon segments. (F) Population data showing the differences in length and diameter of $Na_V1.6$-positive segments in mid- to high-frequency NM and NMc regions. Error bar = standard error. Data were adapted from Hong et al.[42,43] NM indicates nucleus magnocellularis.

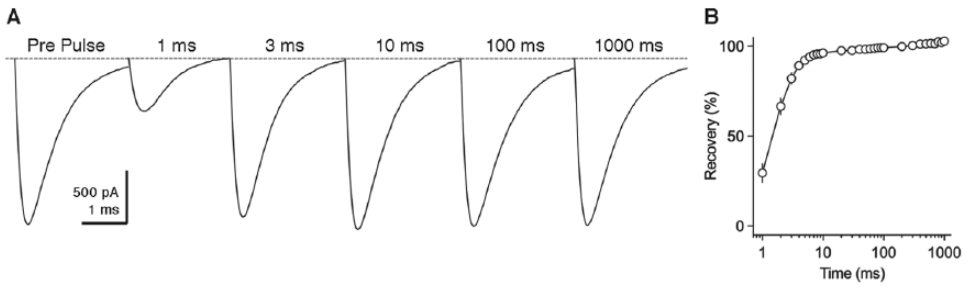

Figure 7. Rapid recovery of transient Na_V current in NM neurons. (A) Representative transient Na_V currents recorded from a mid- to high-frequency NM neuron in response to double-pulse protocol. Neurons were given a pre-pulse to 0 mV, along with the second pulses after varying amount of recovery time (shown above the traces). Recovery time varied from 1 to 1000 ms. (B) Population data showing the recovery ratio (%) as a function of recovery time. Recovery ratio was calculated as the current amplitude at the second pulse normalized to the pre-pulse. Error bar = standard error. Data were recorded using the methods described in Hong et al.[43]

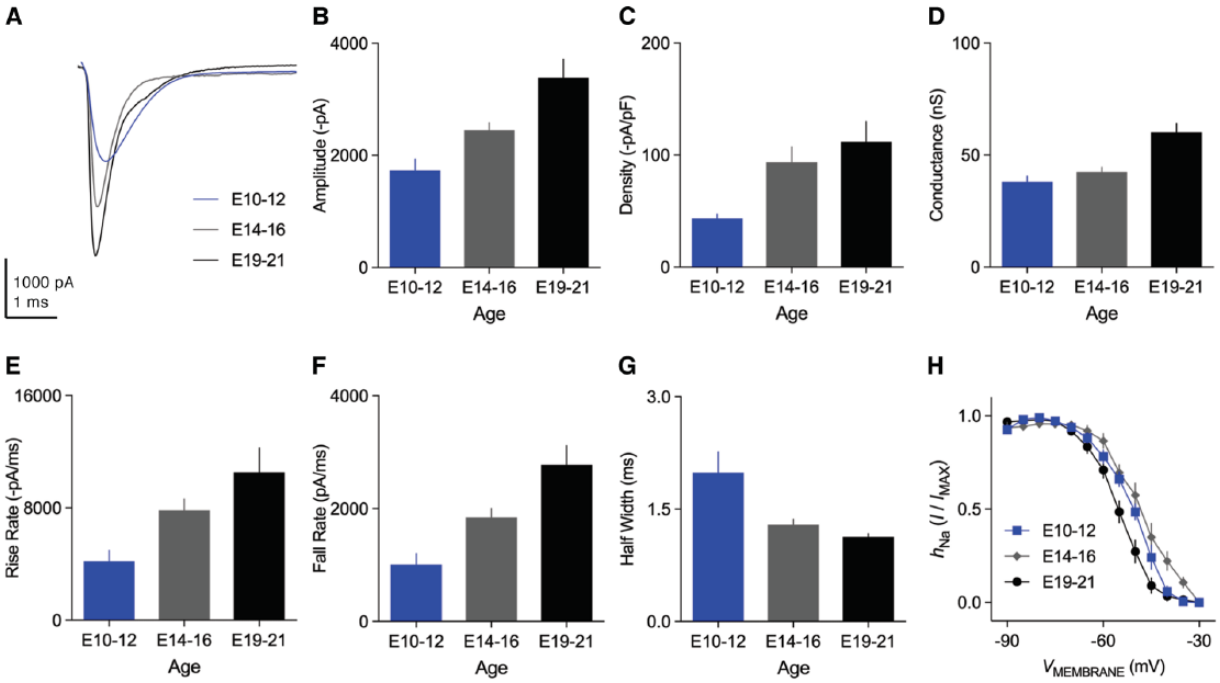

Figure 8. Development of Na_V current properties in NM neurons. (A) Representative transient Na_V currents recorded from mid- to high-frequency NM neurons at E10-E12, E14-E16, and E19-E21. Na_V currents were recorded around the membrane voltage that elicited the maximal current for each age group (−35, −47, and −54 mV, respectively, in this figure). (B-D) Population data showing the development of maximal Na_V current amplitude, density, and conductance. (E-G) Population data showing the development of Na_V current kinetics, ie, rise rate (E), fall rate (F), and half width (G). (H) Population data showing the development of the voltage dependence of Na_V channel inactivation. Error bar = standard error. Data were adapted from Hong et al.[42]

The developmental dominance of $Na_V1.6$ channels in NM neurons, compared with other Na_V channel subtypes (possibly $Na_V1.2$), is biologically relevant. The properties of $Na_V1.6$ channels make it ideal for responding rapidly and repeatedly to high-frequency inputs for several reasons. First, the voltage dependence of activation of $Na_V1.6$ channels favors hyperpolarization compared with $Na_V1.2$ channels,[59] indicating that $Na_V1.6$ channels activate earlier during depolarization. Second, $Na_V1.6$ currents have a lesser degree of use-dependent inactivation compared with $Na_V1.2$ when responding to high-frequency stimulation.[59] This is likely due to $Na_V1.6$ channels' resistance to slow inactivation that progresses with repetitive firing.[60] Third, $Na_V1.6$ channels better promote persistent (I_{NaP}) and resurgent sodium current (I_{NaR}) than other Na_V channel subtypes. $Na_V1.6$ channels mediate significantly larger I_{NaP} than $Na_V1.2$ in both neurons and heterologous expression systems,[59,60] a result also observed for I_{NaR}.[59,61] Furthermore, $Na_V1.6$-knockout mice exhibited reduced I_{NaP} and significantly impaired I_{NaR} in multiple types of neurons.[62–64] It has also been proposed that I_{NaP} functions as an amplifier for subthreshold depolarization[65] and contributes moderately to repetitive AP firing.[66] Interestingly, we also observed an increase in I_{NaP} during development of NM neurons.[50] Finally, I_{NaR} has been widely demonstrated to play an important role in high-frequency AP firing, a ubiquitous property shared across a variety of neuronal types and species.[67] In the following section, we

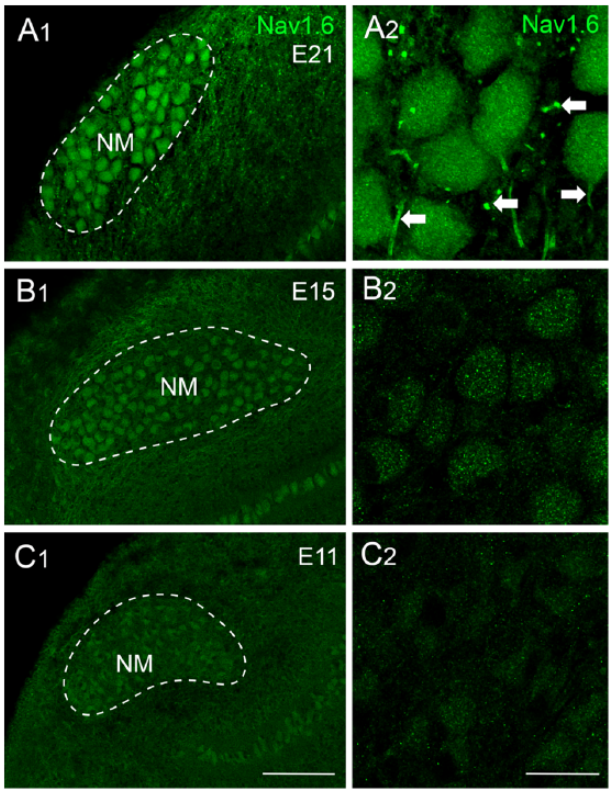

Figure 9. Development of $Na_V1.6$ distribution in NM neurons. (A-C) $Na_V1.6$ immunoreactivity at E21, E15, and E11. Left (A1, B1, and C1) and right (A2, B2, and C2) columns are low- and high-magnification confocal images, respectively. Dashed lines indicate the boundary of NM (mid- to high-frequency). Arrows point to $Na_V1.6$-positive axon segments. Scale bars: 50 μm in C1 (left column) and 10 μm in C2 (right column). Data were taken from Hong et al.[50] NM indicates nucleus magnocellularis.

discuss in detail the properties and function of I_{NaR} in NM neurons.

Properties and function of resurgent sodium current

I_{NaR} has been reported by numerous studies in mammalian neurons that require rapid firing capability, such as cerebellar Purkinje neurons.[67] In terms of the auditory system, this current was observed in spiral ganglion neurons, calyx of Held and neurons in medial nucleus of the trapezoid body.[68–70] Our recent work was the first to report that I_{NaR} is also conserved in chicken NM neurons, with properties and function that resemble those revealed in mammalian neurons.[50] I_{NaR} is the result of specific open-channel blockers auxiliary to α-subunit of Na_V channels. During depolarization (eg, an AP), this open-channel blocker competes with the classic inactivation gate of the channel (ie, the cytoplasmic linker between the III and IV domains of the α-subunit). This blocker is voltage dependent and thus it loses affinity for the α-subunit at repolarized membrane potentials, which results in resurgent flow of sodium ions, known as I_{NaR}.[71] I_{NaR} helps promote AP firing in two ways. First, the competing mechanism between open-channel blocker and the classic inactivation gate reduces the amount of inactivated Na_V channels and thus facilitates the recovery of I_{NaT}. Second, I_{NaR} provides a small depolarizing drive immediately after an AP and thus promotes repetitive firing. The β4-subunit has been proposed as an important candidate for the open-channel blocker in cerebellar Purkinje neurons.[71–74] It is debatable, however, whether the β4-subunit is sufficient and necessary for the generation of I_{NaR}. Studies have shown that the coexpression of the β4-subunit with the Na_V channel α-subunit was not able to induce I_{NaR} in heterologous expression system,[60,75] suggesting additional particles are required. This idea is further supported by the important regulatory roles of fibroblast growth factor homologous factors (FHFs) in the generation of I_{NaR}.[76,77] Moreover, β4-knockout mice showed impaired but not absent I_{NaR} in their Purkinje neurons,[78] suggesting other mechanism(s) contribute to I_{NaR} generation. It is also noteworthy that heterologous expression system transfected with the α-subunit (ie, $Na_V1.6$) alone was able to elicit I_{NaR} with application of specific toxins that caused a "voltage sensor trapping" phenomenon.[79] Regarding the avian auditory system, the molecular substrates for I_{NaR} are not clear; except for the fact that chicken β4-subunit shows conserved amino acid sequence when compared with mammals.[80]

In NM neurons, I_{NaR} can be evoked by applying the same voltage-clamp protocol as in mammalian neurons (Figure 10A, *left*). The depolarizing step that elicits an I_{NaT} prior to repolarization at varying membrane voltages is called as "conditioning step." The current-voltage relationship of I_{NaR} shows a typical "V" shape that peaks at −40 mV (Figure 10B). The maximal amplitude of I_{NaR} depends on the amplitude and length of the conditioning step. Shorter and more positive conditioning steps will result in most of Na_V channels being open channel blocked and thus larger I_{NaR}. Otherwise, Na_V channels are inactivated and require hyperpolarization of the membrane to be released (ie, minimal I_{NaR}). This property is of biological significance, ensuring maximal generation of I_{NaR} after an AP. The kinetics of I_{NaR} can be characterized by two factors: time to peak and decay time constant (tau, Figure 10C). On average, time to peak is ~4 ms and decay time constant ~20 ms when measured at maximal I_{NaR} (Figure 10D). Compared with I_{NaT}, I_{NaR} activates and decays more slowly in NM neurons.

The function of I_{NaR} can be examined both experimentally and computationally.[50,61,71,81] Two voltage-clamp protocols were applied to NM neurons based on the aforementioned conditioning-step-dependent (ie, amplitude and length) generation of I_{NaR}. Nucleus magnocellularis neurons were allowed to recover at rest for varying amounts of time after being exposed to one of two conditions (Figure 11A). In the first condition, most of Na_V channels were open-channel blocked (ie, larger I_{NaR}) by using the conditioning step of +30 mV for 5 ms, while in the second condition, Na_V channels were occupied by the classic inactivation gate (conditioning step of −30 mV for 40 ms). Analysis of two recovery trajectories revealed significantly higher Na_V channel availability and

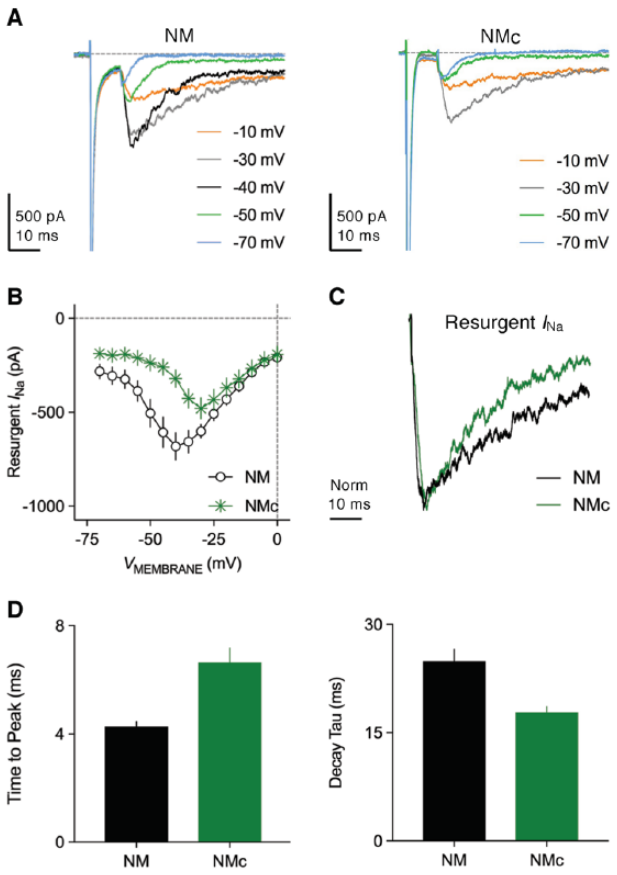

Figure 10. Resurgent sodium current properties. (A) Representative current traces recorded from mid- to high-frequency NM and NMc neurons in response to membrane depolarization to +30 mV (duration = 10 ms) followed by repolarization at varying membrane voltages (indicated in different colors). (B) Population data showing the amplitude of resurgent sodium current as a function of repolarizing membrane voltage ($V_{MEMBRANE}$) for the two neuronal groups. (C) Representative normalized resurgent sodium current traces recorded from mid- to high-frequency NM and NMc neurons. (D) Population data showing the differences in time to peak and decay tau (time constant) of resurgent sodium current between the two neuronal groups. NM indicates nucleus magnocellularis.

shorter recovery time constant (tau) when open-channel blockers were involved (Figure 11B and C). In addition, the increase in Na_V channel availability is more prominent when recovery time is shorter (eg, 2 ms, Figure 11D), which is reminiscent of a highly restricted inter-spike interval during rapid auditory function. Therefore, I_{NaR} helps promote the availability and facilitation of recovery of Na_V channels, which further affects the rapid firing capability of NM neurons. The firing activity of a model NM neuron was characterized with and without I_{NaR} (Figure 12A, *left* and *right*, respectively). In response to square pulse trains of 200 Hz, the model NM neuron with I_{NaR} (Figure 12B and C, *left*, arrow) was able to follow inputs with higher fidelity, as demonstrated by fewer AP failures (Figure 12B, asterisk). Taken together, I_{NaR} plays an important role in regulating the firing activity for NM neurons and is a property conserved between avian and mammalian neurons.

The amplitude of I_{NaR} in NM neurons increases significantly with age. This development, however, does not appear to parallel with the changes in Na_V channel subtypes.[50] The amplitude of I_{NaR} is very small at E11-E12 (before hearing onset, Figure 13A and B) but soon increases to the comparable amount to mature neurons at E14-E16 (during hearing onset, Figure 13C and D). As mentioned above, $Na_V1.6$, a subtype widely expressed in mature NM neurons, only showed weak cytoplasmic staining at these two age groups (see Figure 9). This result suggests that multiple α-subunits are capable of mediating I_{NaR} during development of NM neurons. Indeed, previous studies in mammalian neurons have proposed $Na_V1.2$, 1.5, 1.6, and 1.7 as potential I_{NaR} carriers.[59,82] In addition, changes in β-subunit can also affect the development of I_{NaR}, and thus, all of these possible mechanisms in NM require further investigation.

Tonotopic Heterogeneity of K_V and Na_V Channels in NM

Recent findings demonstrated that NMc neurons located in the low-frequency region present with distinct intrinsic properties and appear to function differently from mid- to high-frequency NM neurons.[19,43] The firing activity and excitability of NMc neurons are notably different from the rest of NM neurons. In response to sustained current injection, NMc neurons are able to fire repetitively, while mid- to high-frequency NM neurons fire a single-onset AP (Figure 3D and F). NMc neurons require significantly reduced amount of threshold current to fire APs. When comparing properties of individual APs, NMc neurons display reduced kinetics and reliability, as demonstrated by smaller fall rate, wider half width and larger jitter (Figure 3E). In terms of passive membrane properties, NMc neurons show more depolarized RMP, longer time constant, and higher input resistance (Figure 3G). They also have larger membrane capacitance, probably as a result of their extensive dendritic processes compared with adendritic NM neurons (see Figure 2A). These differences in NMc neurons are due to their distinct K_V and Na_V current properties (including I_{NaR}), described in detail as follows.

NMc neurons show a significantly reduced amount of total K_V current with maximum amplitude up to ~3 nA at a membrane voltage of +20 mV (Figure 3A and B). In particular, K^+_{HVA} current takes up ~70% of total current at this membrane voltage, while K^+_{LVA} current is ~25%. This is in stark contrast to mid- to high-frequency NM neurons, which show comparable amounts of K^+_{HVA} and K^+_{LVA} currents (Figure 3C). Surprisingly, K_V2 subunits, a K^+_{HVA} component that was not observed in mid- to high-frequency NM, mediates ~30% of total K_V current in NMc neurons (Figure 3C). Consistent with these results, immunochemical experiments showed weaker staining of $K_V3.1$ and $K_V1.1$ protein in NMc region.[26,46] Conversely, expression pattern of $K_V1.2$ mRNA does not show a tonotopic gradient.[26] Furthermore, our recent immunochemical data confirmed the

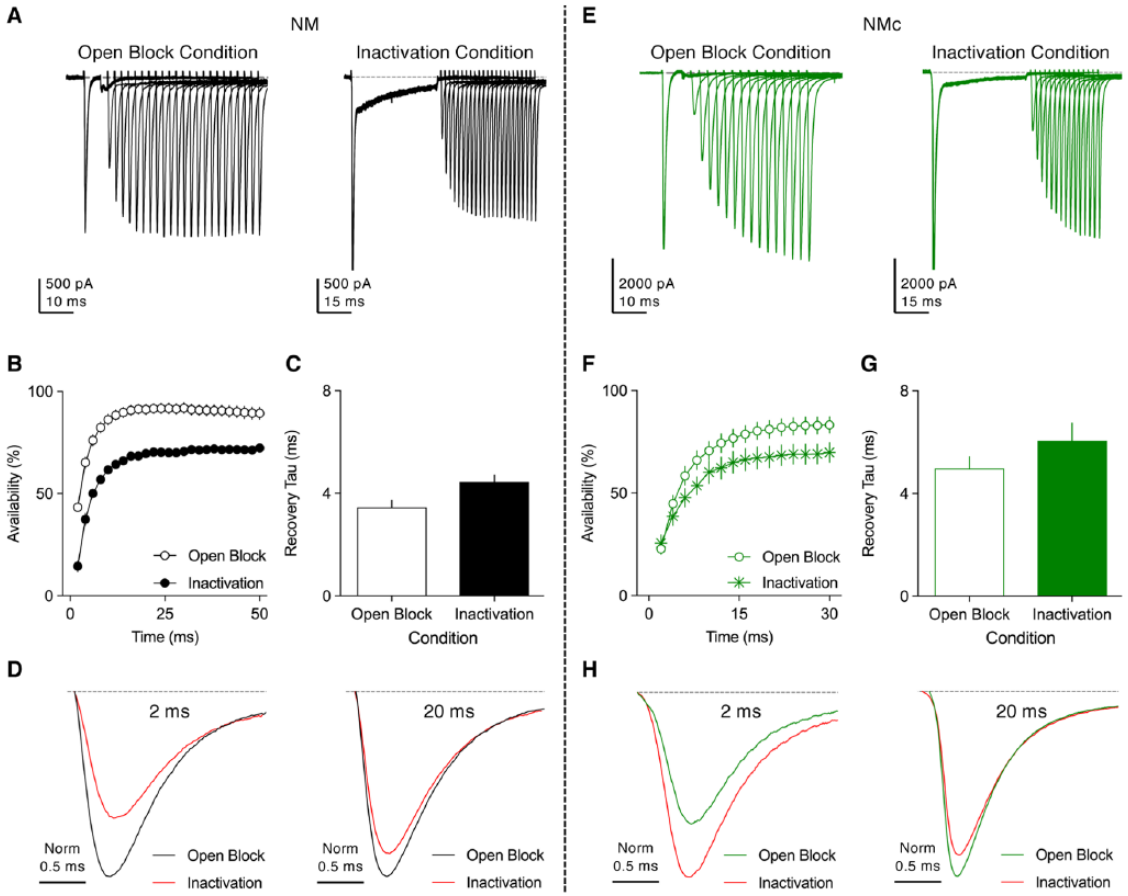

Figure 11. Resurgent sodium current promotes the recovery of Na_V channels. (A and E) Representative current traces recorded from mid- to high-frequency (A) NM and (E) NMc neurons, in response to two voltage-clamp protocols (for details, please refer Hong et al.[43,50]). In short, a conditioning step was applied to neurons followed by recovery period at rest for the varying amounts of time. After recovery, a pulse to 0 mV was applied to evoke a transient Na_V current. The conditioning step is +30 mV at 5 ms in Open-Block Condition and −30 mV at 40 ms in Inactivation Condition. Recovery time varied from 2 to 50 ms for mid- to high-frequency NM neurons and from 2 to 30 ms for NMc neurons. (B and F) Population data showing the Na_V channel availability (%) as a function of recovery time. To calculate Na_V channel availability, a reference pulse to 0 mV was applied to neurons (not shown in the figure), and the amplitude of transient Na_V current after the recovery was normalized to this "reference amplitude." The recovery trajectory was fit by a single exponential, to obtain recovery tau (time constant). (C and G) Population data showing the recovery tau under two different condition states. Error bar = standard error. (D and H) Representative Na_V current traces taken from respective (A) and (E) were normalized and overlaid for recovery time periods of 2 and 20 ms. Data were adapted from Hong et al.[43,50] NM indicates nucleus magnocellularis.

expression of $K_V2.2$ proteins in NMc neurons.[43] Therefore, on one hand, increased K_V2 but reduced K_V3 subunits result in lower level of K^+_{HVA} channels in general, which leads to slower AP kinetics of NMc neurons. On the other hand, reduced K^+_{LVA} channels (mainly K_V1 subunits) are responsible for enhanced excitability and higher input resistance.

Both I_{NaT} and I_{NaR} show substantial differences between mid- to high-frequency NM and NMc neurons. NMc neurons have significantly larger I_{NaT} with faster falling phase than mid- to high-frequency NM neurons (Figure 6A and B). The voltage dependence of the I_{NaT} inactivation curve for NMc neurons is steeper and shifts toward depolarization, as demonstrated by their less negative $V_{1/2}$ ~48 mV and smaller slope factor (k) ~3.7 mV (Figure 6C, *bottom*, and D). In contrast to the increase in I_{NaT}, significantly smaller I_{NaR} was observed in NMc neurons (Figure 10A, *right* and B). The activation of I_{NaR} also shifts in its voltage dependence, as shown by its peak voltage at −30 mV (instead of −40 mV for mid- to high-frequency NM neurons, Figure 10B). The kinetics of I_{NaR} differs significantly between two neuronal groups, but in opposite ways. NMc neurons show longer time to peak but shorter decay time constant (Figure 10C and D). Interestingly, these differences in I_{NaT} and I_{NaR} do not appear to result from different expression of Na_V channel subtypes across tonotopic axis, because robust $Na_V1.6$-positive axon segments were observed throughout the nucleus (Figure 6E). Nevertheless, $Na_V1.6$-positive axon segments in NMc are significantly longer and wider compared with other regions of NM, which in part explains larger I_{NaT} amplitude (Figure 6F). A similar trend was also observed in NL.[58] The tonotopic heterogeneity of β-subunits may be another possibility to explain these differences; however, there is insufficient evidence to draw any conclusion.

I_{NaR} in NMc neurons functions similarly to mid- to high-frequency NM neurons, but somewhat to a different extent.

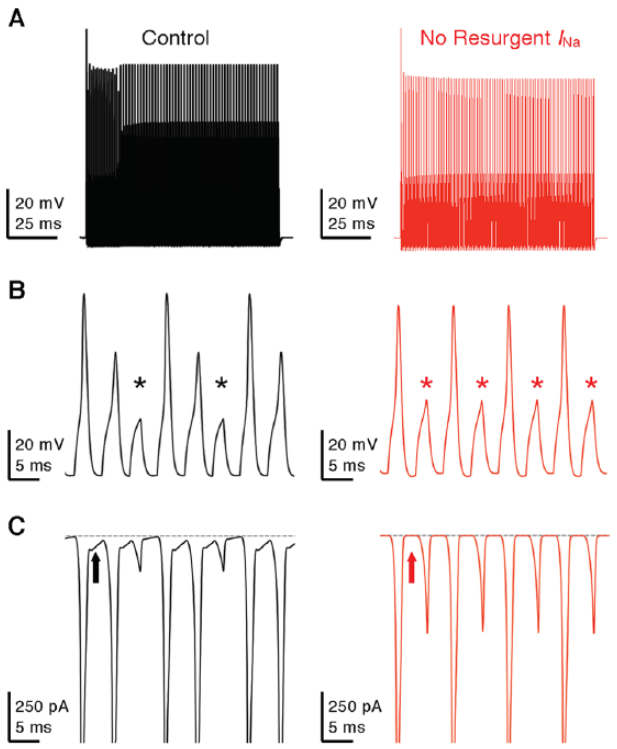

Figure 12. Resurgent sodium current promotes AP firing in model NM neuron. (A) Simulated membrane responses to square pulse trains of 200 Hz in control and with removal of resurgent sodium current. (B) Enlargement of the simulated membrane responses from (A). Asterisks denote AP failures. (C) Simulated Na_V current traces underlying the membrane responses shown in (B). Arrows indicate the generation (left) or elimination (right) of resurgent sodium current.

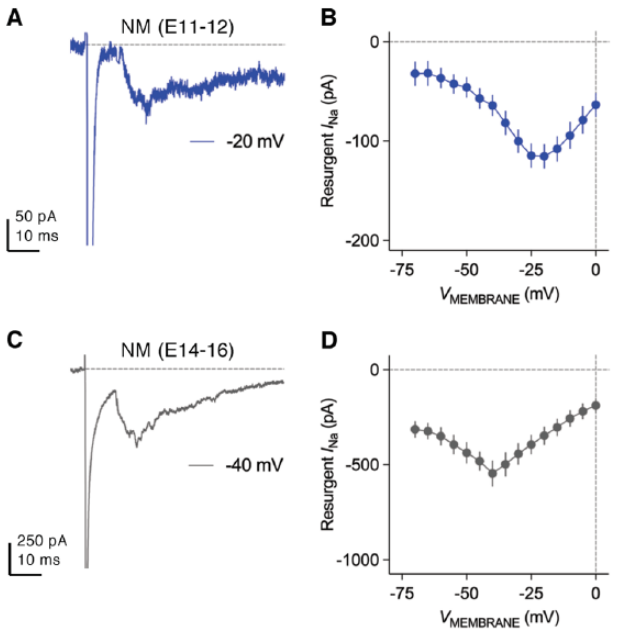

Figure 13. Development of resurgent sodium current in NM neurons. (A and C) Representative current traces recorded from mid- to high-frequency NM neurons at (A) E11-E12 and (C) E14-E16. Repolarizing membrane voltage is (A) –20 mV and (C) –40 mV. (B and D) Population data showing the amplitude of resurgent sodium current as a function of repolarizing membrane voltage ($V_{MEMBRANE}$) at (B) E11-E12 and (D) E14-E16.

For example, the aforementioned two voltage-clamp protocols were also applied to NMc neurons, and recovery trajectories were plotted under the two conditions (Figure 11E and F). The difference in Na_V channel availability became significant beyond the recovery time of 4 ms. Open-channel blockers also shortened the recovery time constant (Figure 11G). Therefore, I_{NaR} also plays an important role in promoting Na_V channel recovery for NMc neurons. When comparing between NMc and adendritic NM neurons, however, there is a noticeable difference in the results. No increase in Na_V channel availability under Open Block Condition was observed for NMc neurons with short recovery time (eg, 2 ms), but the increase becomes evident when recovery time gradually extends (eg, 20 ms, Figure 11H). On the contrary, the effect of I_{NaR} is most prominent at short recovery time for mid- to high-frequency NM neurons (Figure 11D). This observation, along with reduced amount of K_V current, suggests a limitation of NMc neurons for performing rapid auditory function.

This idea is partially supported by different frequency-firing patterns to sinusoidal current injections between mid- to high-frequency NM and NMc neurons.[42,43] In response to stimulation frequency varying from 5 to 200 Hz, the two neuronal groups act as band-pass and low-pass filters, respectively. As illustrated in Figure 14A, APs per cycle were calculated as total number of APs divided by the number of sinusoidal cycles and were plotted as a function of input frequency. Adendritic NM neurons are most responsive to frequencies between 50 and 100 Hz and fire optimally at 75 Hz, while NMc neurons show poor firing fidelity to frequencies >50 Hz (Figure 14A and B). Therefore, NMc neurons indeed show limited capability to follow rapid inputs as compared with their higher frequency counterparts.

Another distinct feature of NMc neurons is the generation of burst firing to 5 and 10 Hz sinusoidal current injections, while mid- to high-frequency NM neurons do not generate APs to these stimulations (Figure 14A and B). Underlying this difference is the filtering function of K^+_{LVA} channels that shapes neuron's response to input with slow rising depolarization (eg, 5 Hz sinusoidal current). Mid- to high-frequency NM neurons contain a large amount of K^+_{LVA} channels, which can activate rapidly in response to slight depolarization and shunt the membrane before reaching the threshold for evoking an AP. In NMc neurons, however, this effect is diminished due to weak expression of K^+_{LVA} channels. This mechanism is further confirmed by our modeling study.[83] A model NM neuron started to generate APs to 10 Hz sinusoidal inputs when its K^+_{LVA} conductance was downregulated systematically. Furthermore, NMc neurons were able to burst fire at instantaneous rates between 45 and 75 Hz. This firing pattern is a combined result of the neuron's K^+_{HVA} conductances and I_{NaR}. Blockade of K^+_{HVA} channels in NMc neurons caused a large depolarization of the membrane, reduced the number of APs, and prolonged the interval between APs within each burst (Figure 15A and B). This firing activity was further examined in the model NMc neuron. The removal of I_{NaR} also resulted in

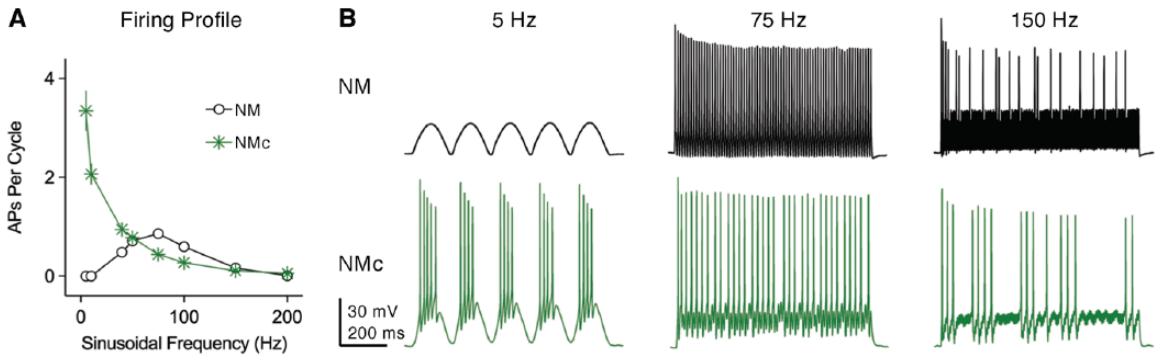

Figure 14. Frequency-firing patterns to sinusoidal current injections. (A) Population data showing APs per cycle as a function of sinusoidal frequency for mid- to high-frequency NM and NMc neurons. APs per cycle were calculated as the number of APs divided by the number of sinusoidal cycles. Error bar = standard error. (B) Representative membrane responses recorded from mid- to high-frequency NM and NMc neurons to sinusoidal current injection with varying frequencies. Data were adapted from Hong et al.[42,43] NM indicates nucleus magnocellularis.

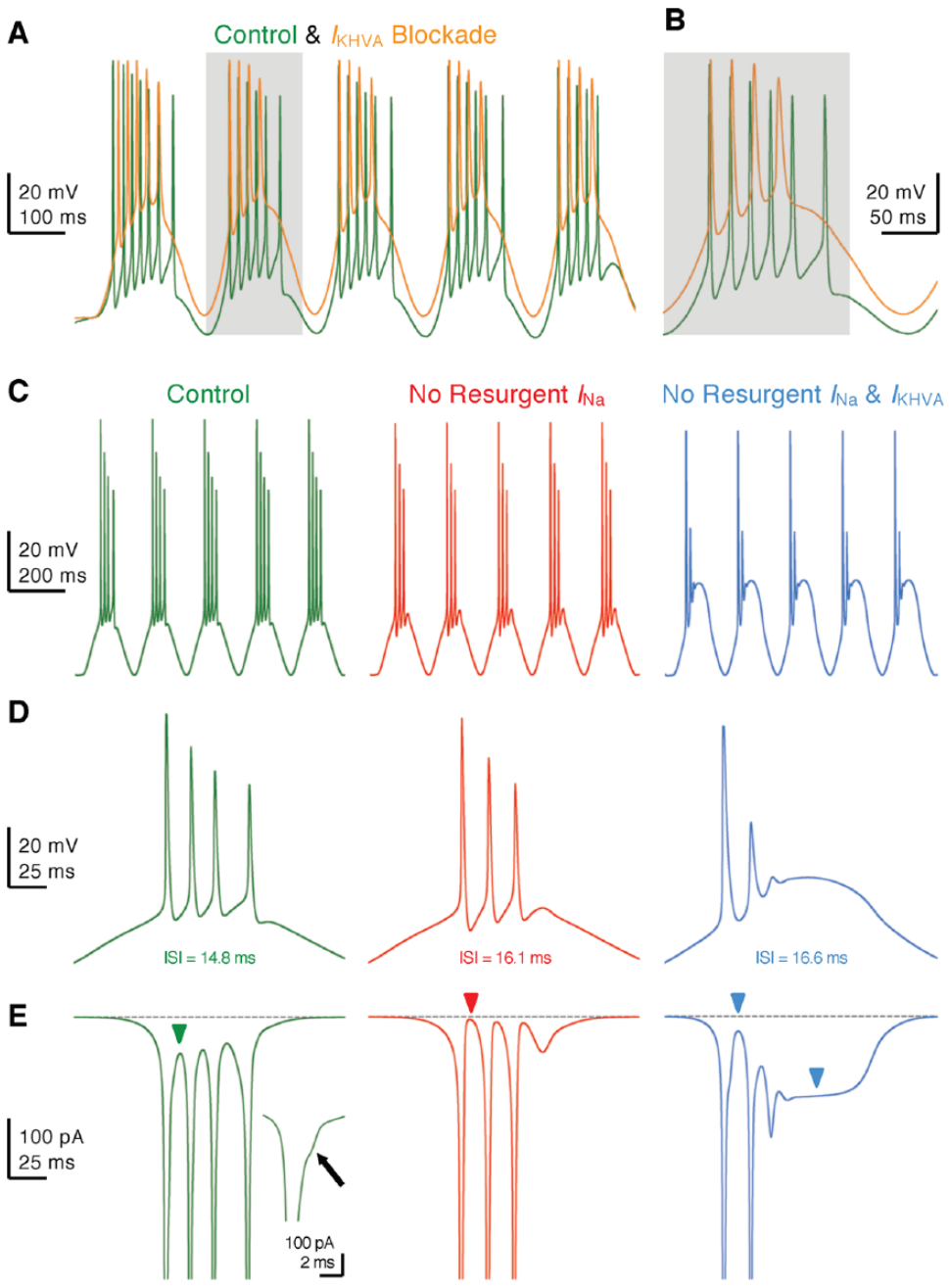

Figure 15. K^+_{HVA} and resurgent sodium current promote burst firing in NMc neurons. (A and B) Representative membrane responses recorded from an NMc neuron to 5 Hz sinusoidal current injections in control and during dual-drug application of Guangxitoxin (GxTx, 100 nM) and TEA to block K^+_{HVA}

Figure 15. (Continued)

channels (I_{KHVA} blockade). Gray area of the second sinusoidal cycle in (A) was expanded and shown in (B). (C) Simulated membrane responses from model NMc neuron to 5 Hz sinusoidal current injections under three conditions: control (*left*), with removal of resurgent sodium current (no resurgent I_{Na}, *middle*) and with removal of both resurgent sodium current and K^+_{HVA} conductances (no resurgent I_{Na} and I_{KHVA}, *right*). (D) The expansion of simulated membrane responses to the first cycle of sinusoidal current injections under three conditions. The inter-spike interval (ISI) represents the time difference between the first and second APs. (E) The expansion of simulated Na_V currents underlying the burst firing shown in (D). Inset showing the enlargement of first AP. Arrow and green arrowhead point to the generation of resurgent sodium current between APs. Red arrowhead points to zero resurgent sodium current. Blue arrowheads point to the generation of persistent sodium current. AP indicates action potential.

weaker burst firing due to a lack of available Na_V channels during subsequent firing (Figure 15C to E, *left* and *middle*). Dual deletion of I_{NaR} and K^+_{HVA} conductances nearly abolished burst firing for the model neuron (Figures 15C to E, *right*). In summary, minimal K^+_{LVA} conductances allow NMc neurons to respond to slow input with burst firing, the pattern of which is regulated synergistically by K^+_{HVA} channels and I_{NaR}.

The responsiveness of NMc neurons to slow input is biologically relevant. Converging inputs from multiple bouton synapses can reduce AP jitter and thus improve phase-locking ability for NMc neurons.[21,29] However, it also results in slower rise phase of EPSP due to the summation process.[21] In addition to input convergence, there is a larger N-methyl-D-aspartate (NMDA)-type glutamate receptor current gradient toward low-frequency NM due to a greater expression of GluN2B-containing receptors.[27] These NMDA receptors generate EPSCs with slow kinetics.[84,85] Therefore, it is plausible that NMc neurons adopt specialized K_V and Na_V channel properties for preserving information contained in slow input, which might eventually be important for processing low-frequency sound. This is in stark contrast to mid- to high-frequency NM neurons, which do not favor input convergence,[29] and thus, their intrinsic properties filter out the slow rising depolarization, in order for optimal response to abrupt depolarization.

Conclusion

The avian auditory brainstem contains structural and functional specializations that impart the ultrafast and temporally precise encoding of sound; a biological process ultimately important for hearing abilities such as sound localization and signal extraction in complex listening environments. In particular, unique K_V, Na_V channel, and I_{NaR} properties play critical roles in shaping the functional phenotype of NM neurons—the avian analogue of bushy cells in the mammalian AVCN. These intrinsic properties undergo profound and specific developmental trajectories. However, both structural and functional specializations in NM show substantial tonotopic heterogeneity that might underlie the diversity of sound-processing mechanisms for different acoustic frequencies.

Acknowledgements

The authors thank George Ordiway for editing a previous version of the manuscript.

Author Contributions

HH performed the experiment shown in Figure 7; HH and JTS wrote the manuscript; Both authors approved the final version for publication.

ORCID iD

Jason Tait Sanchez https://orcid.org/0000-0002-2963-3771

REFERENCES

1. Shannon RV, Zeng FG, Kamath V, Wygonski J, Ekelid M. Speech recognition with primarily temporal cues. *Science*. 1995;270:303–304.
2. Anderson S, Skoe E, Chandrasekaran B, Kraus N. Neural timing is linked to speech perception in noise. *J Neurosci*. 2010;30:4922–4926. doi:10.1523/JNEUROSCI.0107-10.2010.
3. Knudsen EI, Konishi M. Mechanisms of sound localization in the barn owl (Tyto alba). *J Comp Physiol*. 1979;133:13–21. doi:10.1007/bf00663106.
4. Knudsen EI, Blasdel GG, Konishi M. Sound localization by the barn owl (Tyto alba) measured with the search coil technique. *J Comp Physiol*. 1979;133:1–11. doi:10.1007/bf00663105.
5. Carr CE, Konishi M. A circuit for detection of interaural time differences in the brain stem of the barn owl. *J Neurosci*. 1990;10:3227–3246.
6. Koppl C, Carr CE. Low-frequency pathway in the barn owl's auditory brainstem. *J Comp Neurol*. 1997;378:265–282.
7. Sullivan WE, Konishi M. Segregation of stimulus phase and intensity coding in the cochlear nucleus of the barn owl. *J Neurosci*. 1984;4:1787–1799.
8. Gottlieb G. Imprinting in relation to parental and species identification by Avian Neonates. *J Comp Physiol Psychol*. 1965;59:345–356.
9. Gottlieb G. Development of species identification in ducklings: II. Experimental prevention of perceptual deficit caused by embryonic auditory deprivation. *J Comp Physiol Psychol*. 1975;89:675–684.
10. Gottlieb G. Development of species identification in ducklings: V. Perceptual differentiation in the embryo. *J Comp Physiol Psychol*. 1979;93:831–854. doi:10.1037/h0077614.
11. Rubel EW, Parks TN. Organization and development of brain stem auditory nuclei of the chicken: tonotopic organization of n. magnocellularis and n. laminaris. *J Comp Neurol*. 1975;164:411–433.
12. Parks TN, Rubel EW. Organization and development of brain stem auditory nuclei of the chicken: organization of projections from n. magnocellularis to n. laminaris. *J Comp Neurol*. 1975;164:435–448.
13. Smith DJ, Rubel EW. Organization and development of brain stem auditory nuclei of the chicken: dendritic gradients in nucleus laminaris. *J Comp Neurol*. 1979;186:213–239.
14. Young SR, Rubel EW. Frequency-specific projections of individual neurons in chick brainstem auditory nuclei. *J Neurosci*. 1983;3:1373–1378.
15. Kreithen ML, Quine DB. Infrasound detection by the homing pigeon—a behavioral audiogram. *J Comp Physiol*. 1979;129:1–4. doi:10.1007/Bf00679906.
16. Hill EM, Koay G, Heffner RS, Heffner HE. Audiogram of the chicken (Gallus gallus domesticus) from 2 Hz to 9 kHz. *J Comp Physiol*. 2014;200:863–870. doi:10.1007/s00359-014-0929-8.
17. Warchol ME, Dallos P. Neural coding in the chick cochlear nucleus. *J Comp Physiol*. 1990;166:721–734.
18. Koppl C. Phase locking to high frequencies in the auditory nerve and cochlear nucleus magnocellularis of the barn owl, Tyto alba. *J Neurosci*. 1997;17:3312–3321.
19. Wang X, Hong H, Brown DH, Sanchez JT, Wang Y. Distinct neural properties in the low-frequency region of the chicken cochlear nucleus magnocellularis [published online ahead of print April 11, 2017]. *Eneuro*. doi:10.1523/eneuro.0016-17.2017.

20. Warchol ME, Dallos P. Neural response to very low-frequency sound in the avian cochlear nucleus. *J Comp Physiol*. 1989;166:83–95.
21. Kuba H, Ohmori H. Roles of axonal sodium channels in precise auditory time coding at nucleus magnocellularis of the chick. *J Physiol*. 2009;587:87–100. doi:10.1113/jphysiol.2008.162651.
22. Parks TN, Rubel EW. Organization and development of the brain stem auditory nuclei of the chicken: primary afferent projections. *J Comp Neurol*. 1978;180:439–448.
23. Jhaveri S, Morest DK. Sequential alterations of neuronal architecture in nucleus magnocellularis of the developing chicken: a Golgi study. *Neuroscience*. 1982;7:837–853.
24. Jhaveri S, Morest DK. Neuronal architecture in nucleus magnocellularis of the chicken auditory system with observations on nucleus laminaris: a light and electron microscope study. *Neuroscience*. 1982;7:809–836.
25. Ryugo DK, Parks TN. Primary innervation of the avian and mammalian cochlear nucleus. *Brain Res Bull*. 2003;60:435–456.
26. Fukui I, Ohmori H. Tonotopic gradients of membrane and synaptic properties for neurons of the chicken nucleus magnocellularis. *J Neurosci*. 2004;24:7514–7523.
27. Lu T, Trussell LO. Development and elimination of endbulb synapses in the chick cochlear nucleus. *J Neurosci*. 2007;27:808–817. doi:10.1523/JNEUROSCI.4871-06.2007.
28. Jackson H, Parks TN. Functional synapse elimination in the developing avian cochlear nucleus with simultaneous reduction in cochlear nerve axon branching. *J Neurosci*. 1982;2:1736–1743.
29. Oline SN, Ashida G, Burger RM. Tonotopic optimization for temporal processing in the cochlear nucleus. *J Neurosci*. 2016;36:8500–8515. doi:10.1523/JNEUROSCI.4449-15.
30. Koppl C. Auditory nerve terminals in the cochlear nucleus magnocellularis: differences between low and high frequencies. *J Comp Neurol*. 1994;339:438–446. doi:10.1002/cne.903390310.
31. Overholt EM, Rubel EW, Hyson RL. A circuit for coding interaural time differences in the chick brainstem. *J Neurosci*. 1992;12:1698–1708.
32. Joseph AW, Hyson RL. Coincidence detection by binaural neurons in the chick brain stem. *J Neurophysiol*. 1993;69:1197–1211.
33. Jeffress LA. A place theory of sound localization. *J Comp Physiol Psychol*. 1948;41:35–39.
34. Seidl AH, Rubel EW, Barria A. Differential conduction velocity regulation in ipsilateral and contralateral collaterals innervating brainstem coincidence detector neurons. *J Neurosci*. 2014;34:4914–4919. doi:10.1523/JNEUROSCI.5460-13.2014.
35. Fischer BJ, Seidl AH. Resolution of interaural time differences in the avian sound localization circuit—a modeling study. *Front Comput Neurosci*. 2014;8:99. doi:10.3389/fncom.2014.00099.
36. Seidl AH, Rubel EW, Harris DM. Mechanisms for adjusting interaural time differences to achieve binaural coincidence detection. *J Neurosci*. 2010;30:70–80. doi:10.1523/JNEUROSCI.3464-09.2010.
37. Seidl AH, Rubel EW. Systematic and differential myelination of axon collaterals in the mammalian auditory brainstem. *Glia*. 2016;64:487–494. doi:10.1002/glia.22941.
38. Koppl C. Evolution of sound localisation in land vertebrates. *Curr Biol*. 2009;19:635–639. doi:10.1016/j.cub.2009.05.035.
39. McAlpine D, Jiang D, Palmer AR. A neural code for low-frequency sound localization in mammals. *Nat Neurosci*. 2001;4:396–401. doi:10.1038/86049.
40. Grothe B, Pecka M, McAlpine D. Mechanisms of sound localization in mammals. *Physiol Rev*. 2010;90:983–1012. doi:10.1152/physrev.00026.2009.
41. Koppl C, Carr CE. Maps of interaural time difference in the chicken's brainstem nucleus laminaris. *Biol Cybern*. 2008;98:541–559. doi:10.1007/s00422-008-0220-6.
42. Hong H, Rollman L, Feinstein B, Sanchez JT. Developmental profile of ion channel specializations in the avian nucleus magnocellularis. *Front Cell Neurosci*. 2016;10:80. doi:10.3389/fncel.2016.00080.
43. Hong H, Wang X, Lu T, Zorio DAR, Wang Y, Sanchez JT. Diverse intrinsic properties shape functional phenotype of low-frequency neurons in the auditory brainstem. *Front Cell Neurosci*. 2018;12:175. doi:10.3389/fncel.2018.00175.
44. Koyano K, Funabiki K, Ohmori H. Voltage-gated ionic currents and their roles in timing coding in auditory neurons of the nucleus magnocellularis of the chick. *Neurosci Res*. 1996;26:29–45.
45. Rathouz M, Trussell L. Characterization of outward currents in neurons of the avian nucleus magnocellularis. *J Neurophysiol*. 1998;80:2824–2835.
46. Parameshwaran S, Carr CE, Perney TM. Expression of the Kv3.1 potassium channel in the avian auditory brainstem. *J Neurosci*. 2001;21:485–494.
47. Reyes AD, Rubel EW, Spain WJ. Membrane properties underlying the firing of neurons in the avian cochlear nucleus. *J Neurosci*. 1994;14:5352–5364.
48. Kuba H, Yamada R, Ishiguro G, Adachi R. Redistribution of Kv1 and Kv7 enhances neuronal excitability during structural axon initial segment plasticity. *Nat Commun*. 2015;6:8815. doi:10.1038/ncomms9815.
49. Howard MA, Burger RM, Rubel EW. A developmental switch to GABAergic inhibition dependent on increases in Kv1-type K+ currents. *J Neurosci*. 2007;27:2112–2123.
50. Hong H, Lu T, Wang X, Wang Y, Sanchez JT. Resurgent sodium current promotes action potential firing in the avian auditory brainstem. *J Physiol*. 2018;596:423–443 doi:10.1113/jp275083.
51. Johnston J, Forsythe ID, Kopp-Scheinpflug C. Going native: voltage-gated potassium channels controlling neuronal excitability. *J Physiol*. 2010;588:3187–3200. doi:10.1113/jphysiol.2010.191973.
52. Akter N, Adachi R, Kato A, Fukaya R, Kuba H. Auditory input shapes tonotopic differentiation of Kv1.1 expression in avian cochlear nucleus during late development. *J Neurosci*. 2018;38:2967–2980. doi:10.1523/JNEUROSCI.2472-17.2018.
53. Jones TA, Jones SM, Paggett KC. Emergence of hearing in the chicken embryo. *J Neurophysiol*. 2006;96:128–141. doi:10.1152/jn.00599.2005.
54. Parameshwaran-Iyer S, Carr CE, Perney TM. Localization of KCNC1 (Kv3.1) potassium channel subunits in the avian auditory nucleus magnocellularis and nucleus laminaris during development. *J Neurobiol*. 2003;55:165–178.
55. Saunders JC, Coles RB, Gates GR. The development of auditory evoked responses in the cochlea and cochlear nuclei of the chick. *Brain Res*. 1973;63:59–74.
56. Rebillard G, Rubel EW. Electrophysiological study of the maturation of auditory responses from the inner ear of the chick. *Brain Res*. 1981;229:15–23.
57. Aman TK, Raman IM. Subunit dependence of Na channel slow inactivation and open channel block in cerebellar neurons. *Biophys J*. 2007;92:1938–1951. doi:10.1529/biophysj.106.093500.
58. Kuba H, Adachi R, Ohmori H. Activity-dependent and activity-independent development of the axon initial segment. *J Neurosci*. 2014;34:3443–3453. doi:10.1523/JNEUROSCI.4357-13.2014.
59. Rush AM, Dib-Hajj SD, Waxman SG. Electrophysiological properties of two axonal sodium channels, Nav1.2 and Nav1.6, expressed in mouse spinal sensory neurones. *J Physiol*. 2005;564:803–815. doi:10.1113/jphysiol.2005.083089.
60. Chen Y, Yu FH, Sharp EM, Beacham D, Scheuer T, Catterall WA. Functional properties and differential neuromodulation of Na(v)1.6 channels. *Mol Cell Neurosci*. 2008;38:607–615. doi:10.1016/j.mcn.2008.05.009.
61. Patel RR, Barbosa C, Xiao Y, Cummins TR. Human Nav1.6 channels generate larger resurgent currents than human Nav1.1 channels, but the Navbeta4 peptide does not protect either isoform from use-dependent reduction. *PLoS ONE*. 2015;10:e0133485. doi:10.1371/journal.pone.0133485.
62. Raman IM, Sprunger LK, Meisler MH, Bean BP. Altered subthreshold sodium currents and disrupted firing patterns in Purkinje neurons of Scn8a mutant mice. *Neuron*. 1997;19:881–891.
63. Enomoto A, Han JM, Hsiao CF, Chandler SH. Sodium currents in mesencephalic trigeminal neurons from Nav1.6 null mice. *J Neurophysiol*. 2007;98:710–719. doi:10.1152/jn.00292.2007.
64. Do MTH, Bean BP. Sodium currents in subthalamic nucleus neurons from Na(v)1.6-null mice. *J Neurophysiol*. 2004;92:726–733. doi:10.1152/jn.00186.2004.
65. Eijkelkamp N, Linley JE, Baker MD, et al. Neurological perspectives on voltage-gated sodium channels. *Brain*. 2012;135:2585–2612. doi:10.1093/brain/aws225.
66. Magistretti J, Castelli L, Forti L, D'Angelo E. Kinetic and functional analysis of transient, persistent and resurgent sodium currents in rat cerebellar granule cells in situ: an electrophysiological and modelling study. *J Physiol*. 2006;573:83–106. doi:10.1113/jphysiol.2006.106682.
67. Lewis AH, Raman IM. Resurgent current of voltage-gated Na(+) channels. *J Physiol*. 2014;592:4825–4838. doi:10.1113/jphysiol.2014.277582.
68. Browne L, Smith KE, Jagger DJ. Identification of persistent and resurgent sodium currents in spiral ganglion neurons cultured from the mouse cochlea [published online ahead of print November 14, 2017]. *Eneuro*. doi:10.1523/ENEURO.0303-17.2017.
69. Kim JH, Kushmerick C, von Gersdorff H. Presynaptic resurgent Na+ currents sculpt the action potential waveform and increase firing reliability at a CNS nerve terminal. *J Neurosci*. 2010;30:15479–15490. doi:10.1523/jneurosci.3982-10.2010.
70. Leao, et al. Altered sodium currents in auditory neurons of congenitally deaf mice. 2006 doi: 10.1111/j.1460-9568.2006.04982.x
71. Raman IM, Bean BP. Inactivation and recovery of sodium currents in cerebellar Purkinje neurons: evidence for two mechanisms. *Biophys J*. 2001;80:729–737. doi:10.1016/S0006-3495(01)76052-3.
72. Grieco TM, Malhotra JD, Chen C, Isom LL, Raman IM. Open-channel block by the cytoplasmic tail of sodium channel beta4 as a mechanism for resurgent sodium current. *Neuron*. 2005;45:233–244. doi:10.1016/j.neuron.2004.12.035.
73. Bant JS, Raman IM. Control of transient, resurgent, and persistent current by open-channel block by Na channel beta4 in cultured cerebellar granule neurons. *Proc Natl Acad Sci U S A*. 2010;107:12357–12362. doi:10.1073/pnas.1005633107.
74. Barbosa C, Tan ZY, Wang R, et al. Navbeta4 regulates fast resurgent sodium currents and excitability in sensory neurons. *Mol Pain*. 2015;11:60. doi:10.1186/s12990-015-0063-9.

75. Aman TK, Grieco-Calub TM, Chen C, et al. Regulation of persistent Na current by interactions between beta subunits of voltage-gated Na channels. *J Neurosci*. 2009;29:2027–2042. doi:10.1523/JNEUROSCI.4531-08.2009.
76. Yan H, Pablo JL, Wang C, Pitt GS. FGF14 modulates resurgent sodium current in mouse cerebellar Purkinje neurons. *Elife*. 2014;3:e04193. doi:10.7554/eLife.04193.
77. Barbosa C, Xiao Y, Johnson AJ, et al. FHF2 isoforms differentially regulate Nav1.6-mediated resurgent sodium currents in dorsal root ganglion neurons. *Pflugers Arch*. 2017;469:195–212. doi:10.1007/s00424-016-1911-9.
78. Ransdell JL, Dranoff E, Lau B, et al. Loss of Navbeta4-mediated regulation of sodium currents in adult Purkinje neurons disrupts firing and impairs motor coordination and balance. *Cell Rep*. 2017;19:532–544. doi:10.1016/j.celrep.2017.03.068.
79. Schiavon E, Sacco T, Cassulini RR, et al. Resurgent current and voltage sensor trapping enhanced activation by a beta-scorpion toxin solely in Nav1.6 channel. Significance in mice Purkinje neurons. *J Biol Chem*. 2006;281:20326–20337. doi:10.1074/jbc.M600565200.
80. Lewis AH, Raman IM. Cross-species conservation of open-channel block by Na channel beta4 peptides reveals structural features required for resurgent Na current. *J Neurosci*. 2011;31:11527–11536. doi:10.1523/JNEUROSCI.1428-11.2011.
81. Khaliq ZM, Gouwens NW, Raman IM. The contribution of resurgent sodium current to high-frequency firing in Purkinje neurons: an experimental and modeling study. *J Neurosci*. 2003;23:4899–4912.
82. Jarecki BW, Piekarz AD, Jackson JO 2nd, Cummins TR. Human voltage-gated sodium channel mutations that cause inherited neuronal and muscle channelopathies increase resurgent sodium currents. *J Clin Invest*. 2010;120:369–378. doi:10.1172/JCI40801.
83. Lu T, Wade K, Hong H, Sanchez JT. Ion channel mechanisms underlying frequency-firing patterns of the avian nucleus magnocellularis: a computational model. *Channels (Austin)*. 2017;11:444–458. doi:10.1080/19336950.2017.1327493.
84. Sanz-Clemente A, Nicoll RA, Roche KW. Diversity in NMDA receptor composition: many regulators, many consequences. *Neuroscientist*. 2013;19:62–75. doi:10.1177/1073858411435129.
85. Sanchez JT, Wang Y, Lu Y, et al. Nucleus laminaris. In: G. Shepherd & D. D. Addona (eds) *Handbook of Brain Microcircuits Second Edition*. New York, NY: Oxford University Press; 2018:425–436.